36. Pulinets, S. A. and Ouzounov, D., Lithosphere–atmosphere–ionosphere coupling (LAIC) model: an unified concept for earthquake precursors validation. *J. Asian Earth Sci.*, 2011, **41**(4-5), 371–382.
37. Ouzounov, D. *et al.*, Integrated sensing, analysis and validation of atmospheric signals associated with major earthquakes. *Geophys. Res. Abstr., European Geopphys. Union General Assembly*, 2011, **13**, EGU2011-11932-1.
38. Ohring, G. and Gruber, A., Satellite radiation observations and climate theory. *Adv. Geophys.*, 1982, **25**, 237–304.
39. Gruber, A. and Krueger, A., The status of the NOAA outgoing longwave radiation dataset. *Bull. Am. Meteorol. Soc.*, 1984, **65**, 958–962.
40. Ouzounov, D., Pulinets, S. A., Romanov, A., Romanov, A., Tsybulya, K., Davidenko, D., Kafatos, M. and Taylor, P., Atmosphere–ionosphere response to the *M*9 Tohoku earthquake revealed by multi-instrument space-borne and ground observations: preliminary results. *Earthquake Sci.*, 2011, **24**(6), 557–564.
41. Pulinets, S. A. and Boyarchuk, K. A., *Ionospheric Precursors of Earthquakes*, Springer, Berlin, 2004, p. 316.
42. Toutain, J. P. and Baubron, J. C., Gas geochemistry and seismotectonics: a review. *Tectonophysics*, 1998, **304**, 1–27.
43. Omori, Y., Yasuoka, Y., Nagahama, H., Kawada, Y., Ishikawa, T., Tokonami, S. and Shinogi, M., Anomalous radon emanation linked to preseismic electromagnetic phenomena. *Nat. Hazards Earth Syst. Sci.*, 2007, **7**, 629–635.
44. Ondoh, T., Investigation of precursory phenomena in the ionosphere, atmosphere and groundwater before large earthquakes of $M > 6.5$. *Adv. Space Res.*, 2009, **43**, 214–223.
45. Prasad, B. S. N., Nagaraja, T. K., Chandrashekara, M. S., Paramesh, L. and Madhava, M. S., Diurnal and seasonal variations of radioactivity and electrical conductivity near the surface for a continental location Mysore, India. *Atmos. Res.*, 2005, **76**, 65–77.
46. Pulinets, S. A., Ouzounov, D., Karelin, A., Boyarchuk, K. and Pokhmelnykh, L., The physical nature of thermal anomalies observed before strong earthquakes. *Phys. Chem. Earth*, 2006, **31**, 143–153.
47. Pulinets, S. A., Kotsarenko, A. N., Ciraolo, L. and Pulinets, I. A., Special case of ionospheric day-to-day variability associated with earthquake preparation. *Adv. Space Res.*, 2007, **39**, 970–977.
48. Cervone, G., Maekawa, S., Singh, R. P., Hayakawa, M., Kafatos, M. and Shvets, A., Surface latent heat flux and night time LF anomalies prior to the $Mw = 8.3$ Tokachi-Oki earthquake. *Nat. Hazards Earth Syst. Sci.*, 2006, **6**, 109–114.
49. Jun, L., Yi-Chun, Y., Quan, G., Hao-Nan, F. and Peng-Xiao, T., Anomalous Infrasonic waves before a small earthquake in Beijing. *Chin. J. Geophys.*, 2012, **55**(5), 580–586.
50. ReVelle, D. O., Earthquake depth predictions using infrasonic waves. In Proceedings of 28th Seismic Research Review, 2006, pp. 936–946.

ACKNOWLEDGEMENTS. We thank the Physical Sciences Division of NOAA (http://www.cdc.noaa.gov) for providing OLR data and the anonymous reviewers for providing valuable inputs, that helped improve the manuscript. N.V. also thanks SASTRA University for encouragement to carry out the research project.

Received 30 September 2013; revised accepted 1 April 2014

Impact of assimilation of Megha-Tropiques ROSA radio occultation refractivity by observing system simulation experiment

C. J. Johny* and V. S. Prasad

National Centre for Medium Range Weather Forecasting, Noida 201 309, India

Numerical weather prediction models are assimilating more Global Positioning System Radio Occultation (GPSRO) observations into their operational model in recent times as a result of significant positive impact with use of GPSRO data in assimilation system. The Megha-Tropiques satellite mission is aimed to provide large number of observations over the tropical region and carries payload ROSA for providing GPSRO observations. At present, the quality of processed GPSRO retrievals from Megha-Tropiques ROSA is not satisfactory. In order to assess the impact of assimilation of good-quality ROSA observations, an observing system simulation system experiment (OSSE) was conducted using NCMRWF T574 model. The experiment was conducted for a period of 15 days during September 2012 and refractivity operator was used for assimilation. Results show significant improvement in forecast skill for forecasts beyond 72 h with OSSE data.

Keywords: Assimilation system, forecast skill, numerical models, weather prediction.

MEGHA-TROPIQUES is an Indo-French joint satellite mission for studying the water cycle and energy exchanges in the tropics. It is orbiting the Earth at low orbit (~800 km) and low inclination (20°) to provide higher satellite repetivity at lower latitudes. It carries four payloads – SAPHIR, SCRAB, Radio Occultation Sounding of Atmosphere (ROSA) and MADRAS, and can measure rainfall, water vapour and radiation. Many interactions among radiation, water vapour, clouds, precipitation and atmospheric motion determine the life cycle of convective cloud systems, and the occurrence of extreme events like tropical cyclones, monsoons, flood and droughts. Due to dynamic nature of the above parameters, the frequency of observation from low-orbiting Sun-synchronous orbits is inadequate. Only geo-stationary satellites allow continuous monitoring of the tropics, but their visible–IR sensors give limited information on the cloud surface properties or horizontal distribution of water vapour. Low-orbiting satellites with low inclinations can provide more observations at lower latitudes. An inclination at 20° provides six observations of each point on the Inter-Tropical Convergence Zone (ITCZ). The most energetic tropical systems,

*For correspondence. (e-mail: cjjohny@gmail.com)

such as the cloud clusters of ITCZ, the monsoon systems and the tropical cyclones, extend over hundreds of kilometres. Hence, a ground resolution of about 10 km is adequate for these observations. Megha-Tropiques is giving 3–5 passes each day for the tropics.

Global Positioning System Radio Occultation (GPSRO) is a limb-sounding technique which can provide observations at high vertical resolution and minimally affected by clouds, aerosol and precipitation. It has the advantage of uniform coverage over land and ocean, no satellite-to-satellite bias and does not require bias correction in assimilating into numerical weather prediction models. GPSRO observations can be used to anchor the model, avoiding drift to its own climatology. In GNSS limb-sounding hardware is relatively cheap and the data are stable over time. GPSRO data are provided by receivers on-board the Low Earth-Orbiting (LEO) satellites[1]. As the radio signals transmitted by the GPS satellites pass through the atmosphere, they are refracted because of the density gradients along the path. As an LEO satellite sets or rises behind the Earth's limb relative to the GPS transmitter satellite, the on-board GPS receiver takes measurements of the phase and amplitude of the GPS signals. These phase measurements are the relevant fundamental observables and, together with the precise knowledge of the positions and velocities of the GPS and LEO satellites, can be collectively used to derive the inferred atmospheric bending angle as a function of the asymptote miss distance (or 'impact parameter') for each signal under the assumption of spherical symmetry. The contribution of the ionosphere to the bending can be largely removed by using the first-order relationship between the ionospheric refractivity index and the frequency of the signal, and the geometric separation of both rays (L1 and L2) due to the dispersive nature of the ionosphere at the GPS frequencies[2]. Under the assumption of local spherical symmetry, refractivity profiles at the ray perigee point can be derived from bending angle profiles through Abel transform inversions[3]. The usage of GPSRO from LEO was first initiated in 1995 by the GPS/MET experiment[4,5]. At present, operational GPSRO systems like COSMIC, Mettop/GRAS, GRACE-A, SAC-C, C/NOFS and TerraSAR-X together can provide ~2000 profiles a day. Additional GPSRO observations are beneficial, especially when the COSMIC system is now giving far less observations than a few years ago.

Assimilations of the RO retrieved data (refractivity and bending angle) have exhibited promising impact on regional as well as global weather predictions[6–11]. For global models, assimilation of bending angle has the advantage of providing better accuracy, but at the cost of computational expense[7,12]. For regional models, assimilation of refractivity has usually been undertaken using a local observation operator or a nonlocal observation operator[10,13]. GPSRO data have been proven to give a positive impact on some typhoon track and rainfall predictions[13] and the prediction of monsoon-induced rainfall over the western coastal mountain of India[14], based on the control experiment with assimilation of the GPSRO data and the denial experiment without the GPSRO data. Huang *et al.*[15] found some positive impact on regional weather predictions, in majority of case studies by assimilation COSMIC RO refractivity along with other observations. They also observed that in some cases RO assimilation did not show any statistically significant impact. Soundings of GPSRO observations are being assimilated worldwide at most operational NWP centres. In 2007, assimilation of COSMIC GPSRO refractivity observation into GDAF become operational in NCEP[16]. Forecast verifications with respect to its own analysis showed that the impact of GPSRO observation is neutral or slightly negative in the tropics up to day-2 forecast, while improvement is seen in extended range forecast. Improved positive impact upon assimilation is seen on verification against consensus analysis instead of its own analysis. Cucurull[17], with the updated quality control procedures and error characterization for the COSMIC observations, found remarkable improvement in model forecast skill with assimilation of GPSRO data on day-4 forecast, and steadily increases with extended forecast range. In this case also, impact is negligible up to day-2 forecast. Use of bending angle operator in GPSRO assimilation instead of refractivity operator in operational forecast system in NCEP showed slight improvement in dynamic skill of forecast[18]. The study found minute improvement in day-5 geopotential heights and day-3 winds with bending angle operator over refractivity operator.

ROSA is an Italian-made GPS receiver attached with mission for sounding of atmosphere by radio occultation. It has a horizontal resolution of 300 km in the upper troposphere to 150–200 km in the lower troposphere and has vertical resolution of 0.5 km in the lower troposphere to 1.5 km in the lower stratosphere. Spatial coverage of ROSA in the tropical region is much larger than other GPSRO missions. ROSA is able to provide ~300–400 profiles a day. Spatial coverage of ROSA observations in the study period is shown in Figure 1. But comparison studies with COSMIC observations and model forecast (discussed in detail in the next paragraph) showed that at present, the quality of processed ROSA data is poor and attempts to improve the observation quality in near future are in progress. It can be seen from Figure 1 that ROSA gives a large number of observations over the tropical region, which shows that satellite orbital configuration is good. As the quality of processed ROSA data is not satisfactory at present, impact study with the assimilation of these ROSA observations will be a futile exercise. As there are attempts to improve data quality in the near future, an observation system simulation experiment (OSSE) can bring out the real strength of Megha-Tropiques ROSA observation in the forecast system. This attempt is to prove the requirement for works to improve

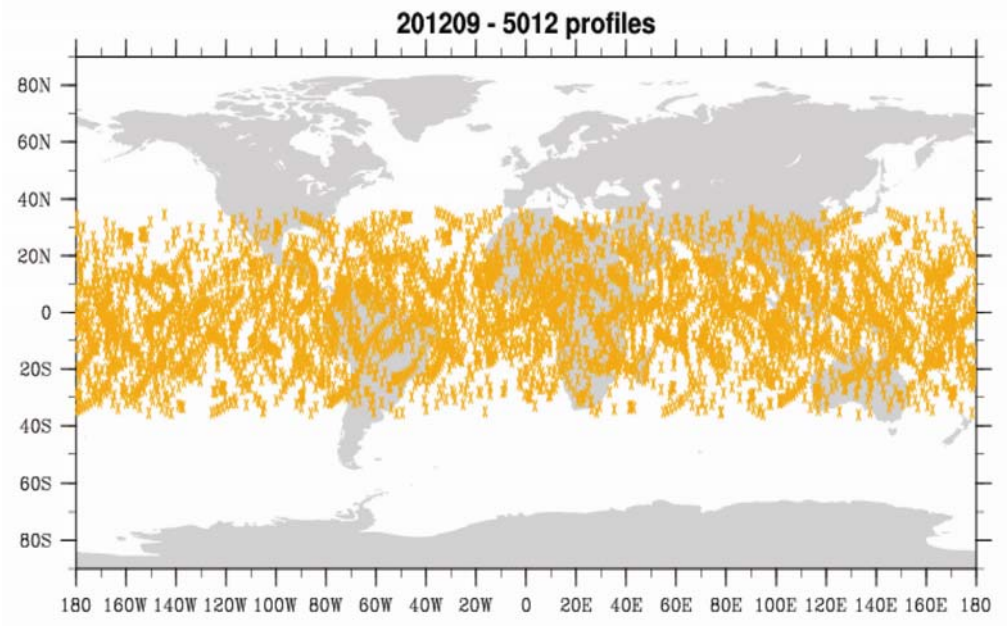

Figure 1. Spatial coverage of ROSA observations for September 2012.

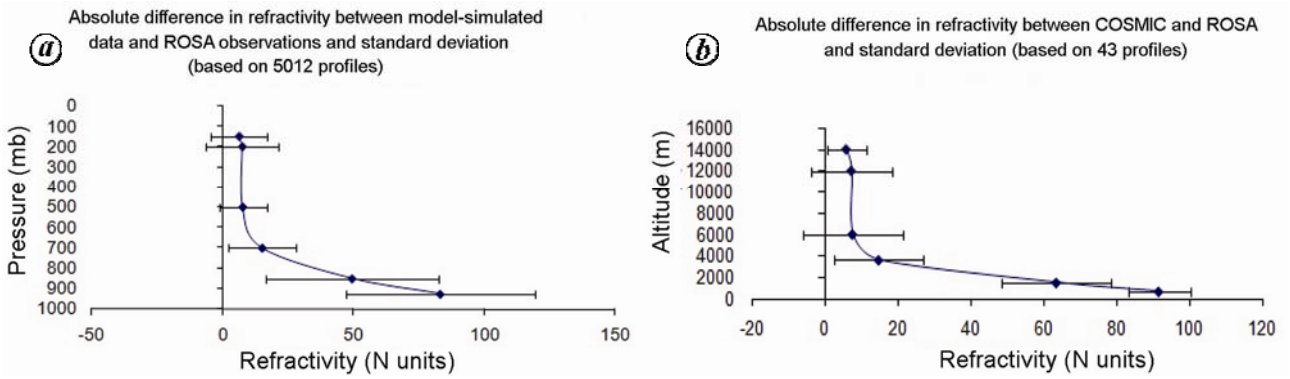

Figure 2. Absolute difference in refractivity between (***a***) ROSA and NCMRWF 574 simulation and (***b***) ROSA and COSMIC.

the ROSA observations quality. Thus observations are simulated using model forecast at ROSA locations and system simulation experiment is conducted using NCMRWF T574 model. To study the impact of ROSA data on rainfall pattern during the monsoon period, the impact experiment was conducted for a period of 15 days from 16 to 31 September 2012. Since GPSRO moisture observations are not up to the mark at lower levels, we chose September for study as moisture is comparatively less during this period of monsoon season and also GPSRO observations are less accurate at lower levels in high moist conditions.

Megha-Tropiques refractivity data were compared with refractivity observations from COSMIC RO and refractivity computed from NCMRWF T574 model. Comparison with COSMIC data was made using the criterion that both observations come within spatial separation of 1° and temporal separation of 1 h. A total of 43 profiles were obtained for comparison based on the above-mentioned criterion. A comparison of the results is shown in Figure 2. Megha-Tropiques refractivity data were also compared with short-range forecast of 6 h made by NCMRWF T574 model four times a day corresponding to 00, 06, 12 and 18 UTC. Comparisons were made as spatial separation of both data are within degree and temporal separation of 1.5 h. As the number of colocated profiles of COSMIC and ROSA is less, we adopted the criterion of spatial separation of 1° for comparison purpose and the criterion of 0.5° separation was used for comparing ROSA and model output as sufficient number of colocated profiles were available. Refractivity was computed from model variables using the formula

$$N = 77.6\, P/T + 3.73 \times 10^5\, e/T^2, \quad (1)$$

where N is the refractivity, T the temperature (K) and e water vapour pressure (mb)[19]. Comparison of the results of 5012 profiles is shown in Figure 2. It can be seen that

the Megha-Tropiques refractivity shows large variation from both COSMIC data and NCMRWF T574 simulated data. Variations are less in the upper levels compared to lower levels. In order to check veracity of using COSMIC and model-simulated data as reference for comparing ROSA observations, inter comparison of COSMIC and model simulated refractivity was performed. Figure 3 shows profile of absolute difference of model-simulated refractivity with COSMIC observations. Comparisons were made with the criterion that both data are within spatial separation of 0.5° and temporal separation of 1.5 h. It can be seen that variation between COSMIC and model-simulated refractivity is within the acceptable limits. At present, the quality of ROSA refractivity data is far from assimilating into the model.

Global Data Assimilation Forecast (GDAF) system based on gridpoint statistical interpolation (GSI) analysis scheme with 3D var assimilation was used in the present experiment. The analysis and forecast were carried out at a horizontal resolution of about 22 km and with 64 levels in vertical. The 3D var cost function used in physical space is given by[20]

$$J = \frac{1}{2}[x^T B^{-1} x + (Hx - o)^T R^{-1} (Hx - o) + J_c], \quad (2)$$

where x is vector of analysis increment, B the background error covariance matrix and o the vector of observational residuals, i.e. $o = o_{obs} - Hx_{guess}$, R the observational covariance matrix, H the transformation operator from analysis variable to observation vector and J_c is dynamical constraint. Details of the analysis and forecast system implemented at NCMRWF can be found in Prasad *et al.*[21], and Dutta and Prasad[22]. Assimilation and forecast were done over the global domain and time window of ±3 h was used for observations. Assimilations were carried out in 6 h time intermittent method. In this method a new estimate of the atmospheric state (analysis) is required every 6 h to initialize a new 9 h global model forecast[23]. Although the background used for each analysis is the previous 6 h forecast, a 9 h forecast is necessary to allow for time interpolation of asynoptic observations that fall within the 6 h analysis time window. The analyses are then used as the initial conditions for subsequent forecasts and the cycle continues. Observations are encoded in NCEP BUFR format and observations of similar types are made into individual files. Different types of conventional (synop, AWS, sonde, buoy, ship, aircraft) and satellite observations (radiance, GPSRO, scatterometer winds, AMV) are assimilated in the model. After performing various quality checks, data are packed into PREPBUFR format. Model variables are converted into pseudo observation variables and observation innovation is computed after applying various quality checks. For satellite radiances, Community Radiative Transfer Model (CRTM) is used to compute pseudo radiance. In the assimilation scheme, iteration method is used to find optimal results. To improve the convergence of cost function (eq. (2)), GSI preconditions it by defining a new variable[20] $y = B^{-1} x$. Then eq. (2) becomes

$$J = y^T B^T y + (HBy - o)^T R^{-1} (HBy - o) + J_c. \quad (3)$$

The gradients of the observation and background part of eq. (2) w.r.t. variable x and eq. (3) w.r.t. variable y minimized iteratively until the gradient is sufficiently minimized or maximum iterations are reached. Variables used in GSI analysis are stream function, unbalanced velocity potential, unbalanced virtual temperature, unbalanced surface pressure, pseudo relative humidity, ozone mixing ratio and cloud condensate mixing ratio.

In GPSRO assimilation algorithms either soundings of retrieved refractivity or bending angle can be used. A forward operator for refractivity is much more easier to implement than bending angle. In this experiment refractivity operator is used for assimilating GPSRO observations. In the assimilation algorithm, geometric height of observation location is converted to geopotential height and model variables of pressure, temperature and specific humidity are interpolated to observation locations and refractivity is computed from interpolated values using forward operator for refractivity (H in eq. (2)) using[24] eq. (4).

$$N = 77.60\frac{P}{T} + 70.4\frac{P_W}{T} + 3.739 \times 10^{-5}\frac{P_W}{T^2}, \quad (4)$$

where P is the pressure of dry air, P_W the water vapour pressure (mb) and T is temperature (K). The algorithm produces increments in refractivity after doing sufficient quality checks and removing the observations above 30 km. Using adjoint of the forward operator increment in refractivity is converted to model variables temperature, pressure and water vapour. Assimilation algorithm produces increments to surface pressure, water vapour

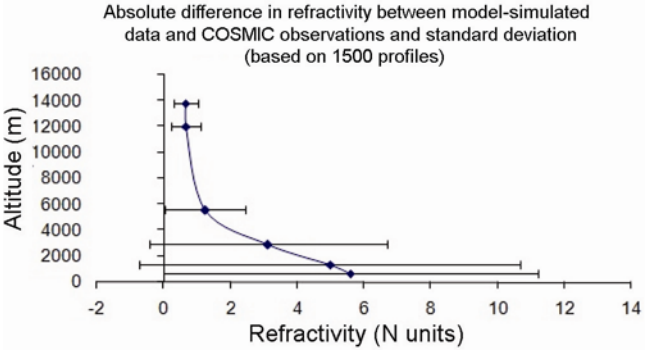

Figure 3. Absolute difference in refractivity between COSMIC and NCMRWF T574 simulation.

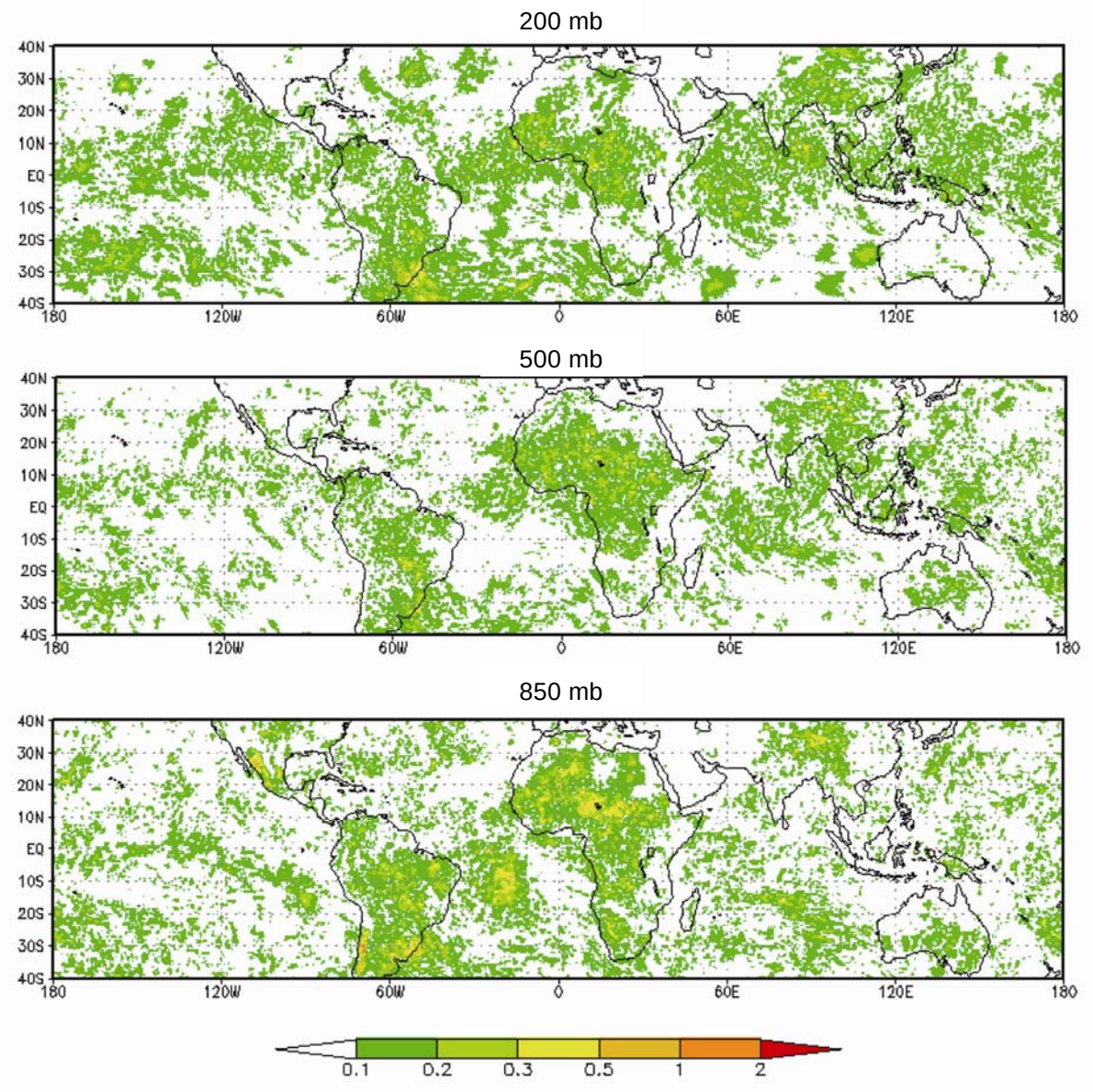

Figure 4. Absolute difference in analysis temperature between experiments GPSRO and T574 averaged over the study period.

levels surrounding observations and to virtual temperature surrounding observations and all levels below it. Two numerical experiments were designed with one control experiment 'T574' without ROSA data and the second 'GPSRO' with model-simulated refractivity values at locations of ROSA measurements. To prepare OSSE data corresponding to ROSA observation locations, six-hourly, short-range forecasts corresponding to 00, 06, 12 and 18 UTC were used. In preparing OSSE data we need to find the nearest model grid point to the location of Megha-Tropiques observation location. The data prepared with the criteria model-simulated values and observations come within the range 0.5° and with temporal difference of ±1.5 h. Eq. (1) was used to calculate refractivity from model variables. OSSE data were prepared and appended to other GPSRO data in NCEP/GDAS BUFR format. Assimilation was performed four times a day corresponding to 00, 06, 12 and 18 UTC and forecasts were done at 00 UTC (05:30 IST) for 5 days. The cyclic assimilation will improve quality of first guess. Time window of ±3 h was used for assimilation of observations. Model evaluation tools (MET) was used to verify the performance of numerical experiments. MET implemented in NCMRWF has been developed by Developmental Testbed Center (DTC), NCEP and performs the analysis at a resolution of 0.5°.

The model forecasts with and without inclusion of ROSA OSSE data were verified against their respective analysis and observations. Impact of assimilation of OSSE data on analysis fields was studied over 40N–40S,

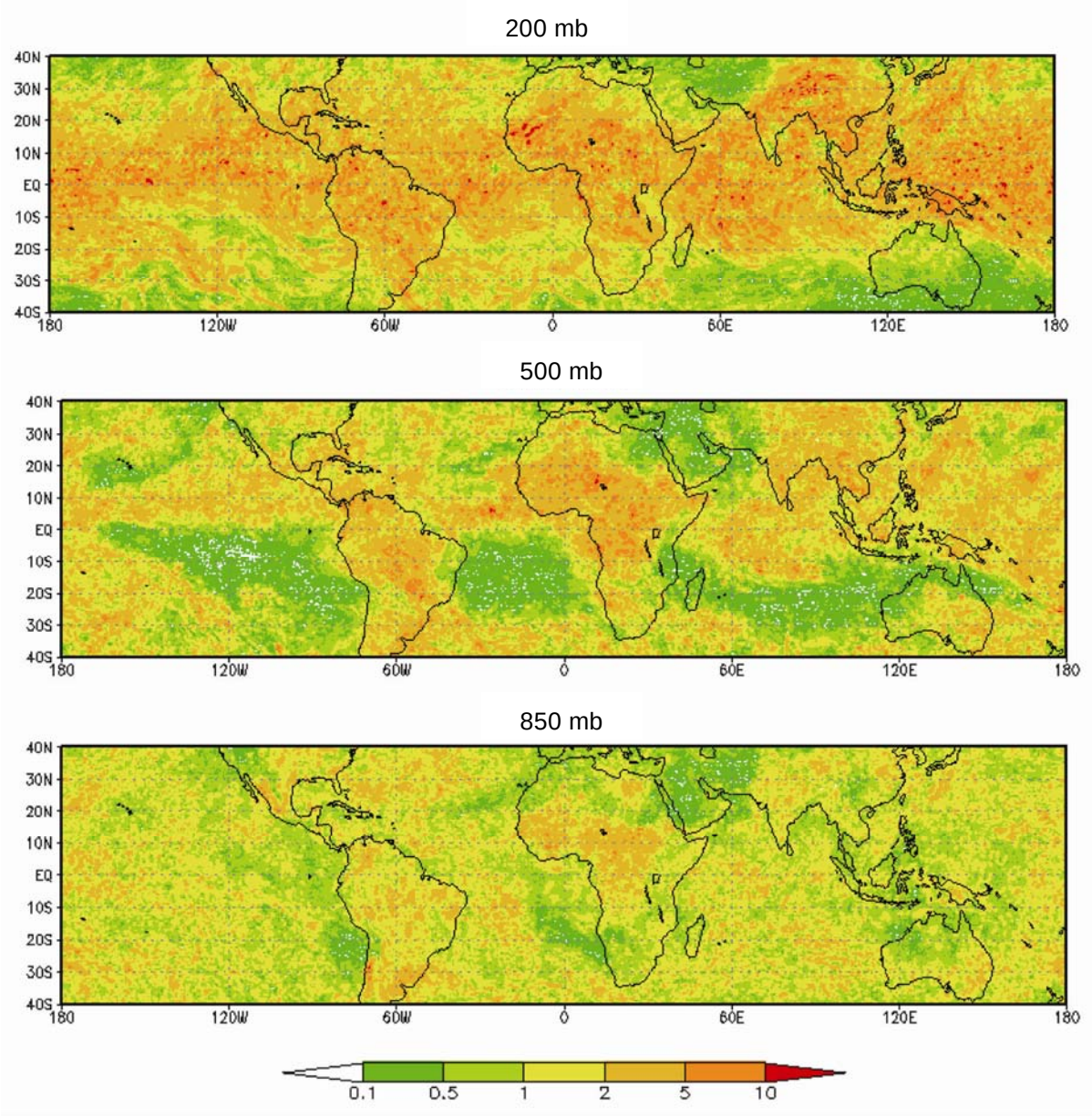

Figure 5. Absolute difference in analysis relative humidity between experiments GPSRO and T574 averaged over the study period.

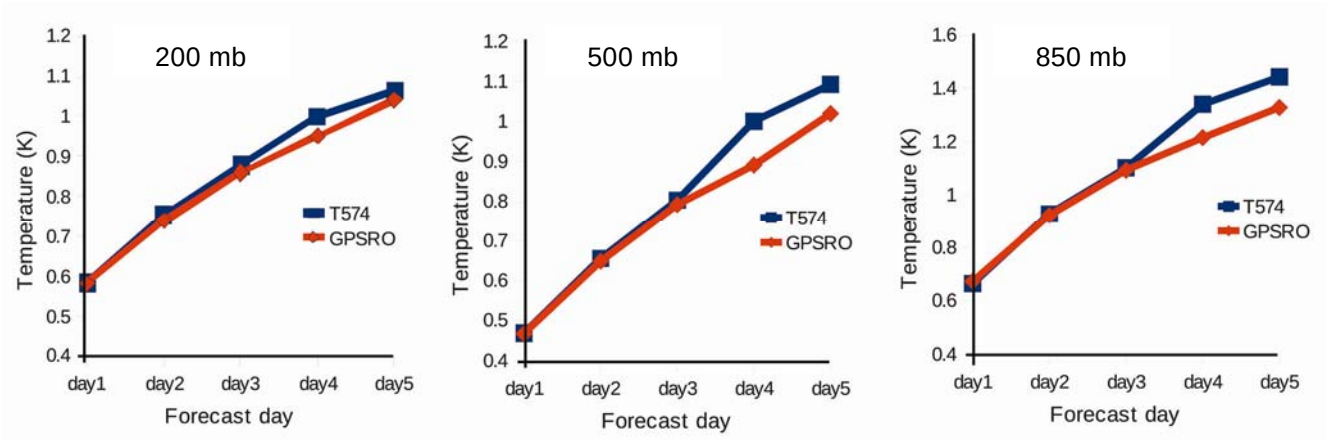

Figure 6. Mean RMSE in temperature w.r.t. analysis at different pressure levels.

Table 1. Showing percentage decrease in RMSE in temperature (T), *U* wind (U), *V* wind (V) and relative humidity (RH)

	200 mb				500 mb				850 mb			
Forecast day	T	U	V	RH	T	U	V	RH	T	U	V	RH
Day-1	0.25	–0.34	–0.57	–1.06	0.27	–1.45	–1.63	–0.26	–1.32	–0.6	–0.75	–0.17
Day-2	1.82	1.2	0.63	1.03	1.08	–0.1	0.25	0.23	0.57	–0.09	–0.15	0.53
Day-3	2.02	1.39	1.24	0.48	1.4	0.27	1.28	0.43	0.78	1.42	0.58	1
Day-4	5.18	6.47	7.35	3.96	10.96	9.84	7.69	4.49	9.32	8.5	7	3.76
Day-5	2.26	3.81	5.4	3.2	6.68	7.39	5.34	4.35	7.97	5.24	4.77	3.36

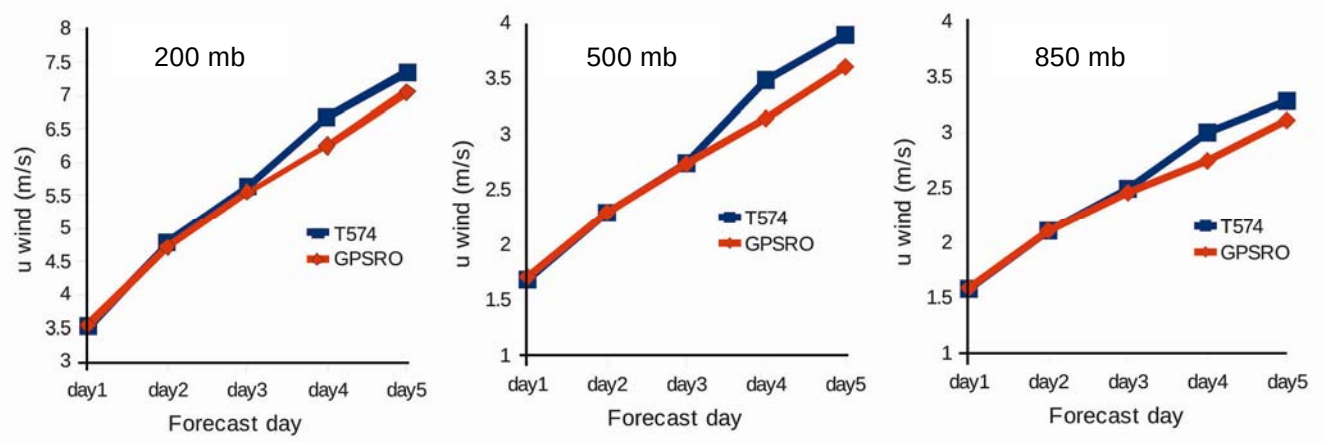

Figure 7. Mean RMSE in zonal wind w.r.t. analysis at different pressure levels.

180E–180W. Figure 4 shows mean absolute difference in the analysis temperature between the two experiments. It can be seen that mean absolute difference in temperature field is less than 0.5 K. Figure 5 shows the mean absolute difference in the analysis relative humidity between two numerical experiments. It can be seen that difference in relative humidity varies up to 10%. It can be seen that over the Indian region mean absolute difference in relative humidity varies between 5% and 10%. Assimilation is not found to induce any particular bias on analysis temperature and humidity (plot not shown).

Model forecasted temperature, relative humidity and wind (*U* and *V* components) were verified against analysis over the tropical region (30N–30S). RMSE was computed for temperature, relative humidity and wind components with respect to their respective analysis at different pressure levels using MET. Mean value of RMSE in temperature corresponding to pressure levels 850, 500 and 200 hpa averaged over the study period is shown in Figure 6. It can be seen from the plots that difference between both the numerical experiments is small and in day-1 forecast impact is positive at 500 and 200 mb (~0.25%) and negative at 850 hpa (–1%). Experiment with simulated OSSE data ('GPSRO') showed improvement over control experiment ('T574') beyond forecasts of day-2 at all pressure levels. Impact of OSSE data can be clearly seen in day-4 and day-5 forecasts. Percentage change in RMSE in temperature, *U* wind, *V* wind and relative humidity with GPSRO experiment is given in Table 1. Mean value of RMSE in *U*-wind and *V*-wind corresponding to pressure levels 850, 500 and 200 hpa averaged over the study period is shown in Figures 7 and 8 respectively. RMSE plots show 'GPSRO' experiment degrades model performance at all pressure levels on day-1 forecast, whereas in day-2 forecast, none of the experiment has clear advantage over other. At 200 hpa pressure level, GPSRO experiment reduces RMSE values of both *U* (1.2%) and *V* (0.63%) components of wind. At 500 hpa, RMSE value of *V* component of wind is reduced (0.28%), whereas *U* component of wind increases (–0.1%) with GPSRO experiment. At 850 mb, GPSRO experiment increases RMSE values of both *U* (–0.09%) and *V* (–0.15) components of wind. With OSSE data model performance shows improvement from day-3 forecast onwards and this can be clearly seen in day-4 and day-5 forecasts. Improvement in RMSE of forecasted *U* and *V* wind can seen in Table 1. Mean RMSE in relative humidity computed for forecast against respective analysis for different pressure levels are given in Figure 9. Difference in RMSE values between the numerical experiments is small and at all pressure levels RMSE values of GPSRO experiment show improvement in forecast skill for forecasts of day-2 to day-5. Improvement in model performance with OSSE data can be clearly seen in day-4 and day-5 forecasts. Quantitative improvement in RMSE of relative humidity with GPSRO experiment is shown in Table 1. Results are similar to impact studies of GPSRO assimilation in operational forecast at

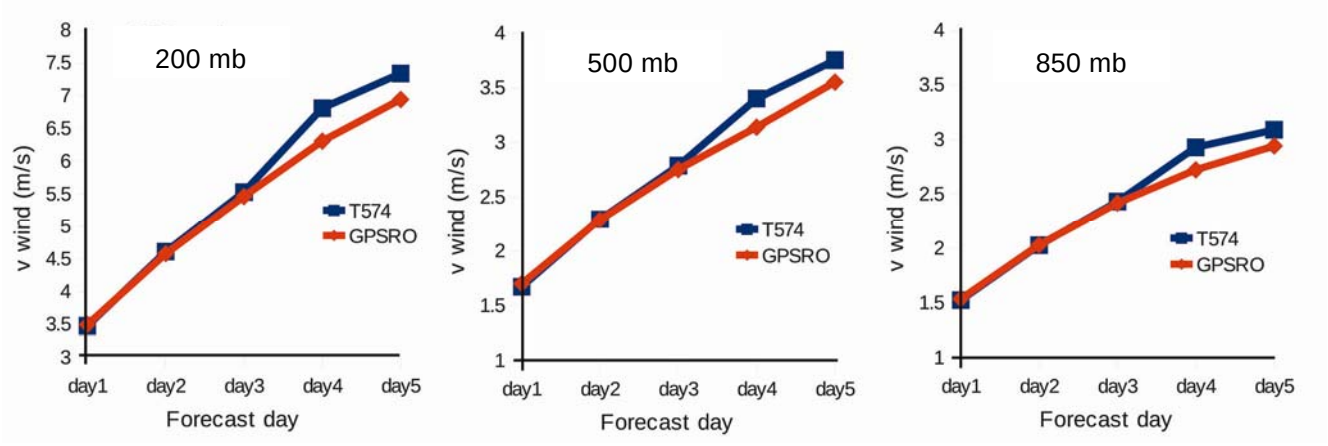

Figure 8. Mean RMSE in meridional wind w.r.t. analysis at different pressure levels.

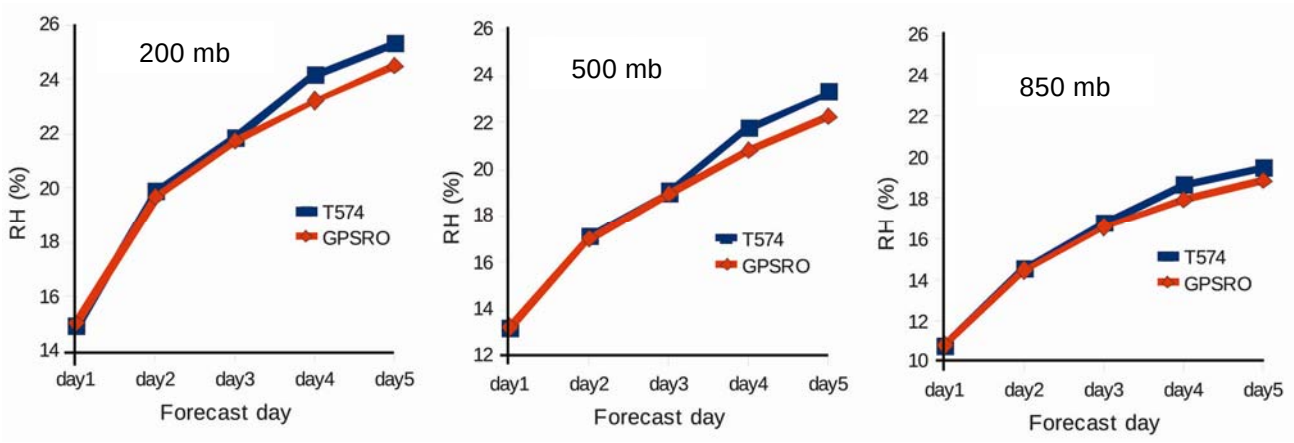

Figure 9. Mean RMSE in relative humidity w.r.t. analysis at different pressure levels.

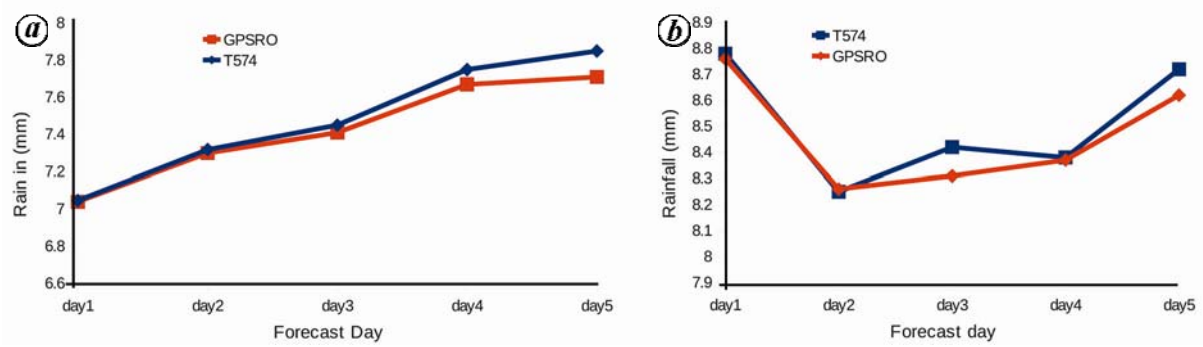

Figure 10. Mean RMSE in 24 h accumulated rainfall with (***a***) IMD-TRMM merged data and (***b***) TRMM data.

NCEP[17,18,20]. In NCEP investigation also noticeable positive impact of assimilation of GPSRO observations is seen only on forecasts beyond day-3 and especially over the tropics slightly negative or neutral impact in day-1 and day-2 forecasts was observed[25]. Improvement in forecast skill was also observed while using consensus analysis of NCEP, UK Met Office and ECMWF analyses instead of only NCEP analysis for verification. There are investigations using regional models in which also GPSRO assimilation degrades performance at shorter scales (less than 2 days), while improvement is seen in the forecast at extended ranges. Using the WRF model, Huang *et al.*[14] found good impact of GPSRO assimilation on 24 and 72 h rainfall forecasts over the west coast of India. Chien and Kuo[26] observed that incorporation of GPSRO data tends to improve the prediction for longer integration, but degrade the forecast at short scales (less than 2 days).

Rainfall verification of model forecast were done against merged gridded rainfall observations of TRMM and IMD gridded TRMM observations. Rainfall verification was done in the latitude range 8–38N and longitude range 68–98E using MET. Figure 10 *a* and *b* shows RMSE plots of forecasted rainfall with merged rainfall observations and TRMM observations respectively. It can be seen that in both cases GPSRO experiment reduces RMSE values.

The performance of both numerical experiments was similar. In general, day-1 and day-2 forecast inclusion of GPSRO–OSSE data degraded the forecast and forecasts beyond day-3 improved model performance in all the inspected variables temperature, wind and relative humidity. In the case of verification of rainfall, experiment with GPSRO–OSSE data showed better performance on all forecast days and improvement was more evident from day-3 onwards. Assimilation of GPSRO observations might improve large-scale features, which in turn impact small-scale features at a later time. In the present experiment positive impact of data was observed in all the investigated parameters beyond day-3 forecasts. The results show the usefulness of data, especially in medium range weather forecasts. OSSE data were prepared by choosing the value at model grid point closer to the observation location. Instead use of weighed average of data at nearest grid points to prepare OSSE data might have given better results.

1. Ware, R. *et al.*, GPS sounding of the atmosphere: Preliminary results. *Bull. Am. Meteorol. Soc*., 1996, **77**, 19–40.
2. Vorobev, V. V. and Krasilnikova, T. G., Estimation of the accuracy of the atmospheric refractive index recovery from Doppler shift measurements at frequencies used in the NAVSTAR system, *Phys. Atmos. Oceans*, 1994, **29**, 602–609.
3. Kuo, Y. H., Wee, T. K., Sokolovskiy, S., Rocken, C., Schreiner, W., Hunt, D, and Anthes, R. A., Inversion and error estimation of GPS radio occultation data. *J. Meteorol. Soc. Jpn.*, 2004, **82**, 507–531.
4. Schreiner, W. S., Hunt, D. C., Rocken, C. and Sokolovskiy, S., Precise GPS data processing for the GPS/MET radio occultation mission at UCAR. In Proceedings of the 1998 National Technical Meeting of the Institute of Navigation, 1998, pp. 103–112.
5. Yunuck, T. P., Liu, C. H. and Ware, R., A history of GPS sounding. *Terr. Atmos. Ocean. Sci.*, 2000, **11**(1), 1–20.
6. Kuo, Y. H., Zou, X. and Huang, W., The impact of GPS data on the prediction of an extratropical cyclone: an observing system simulation experiment. *J. Dyn. Atmos. Ocean*, 1997, **27**, 413–439.
7. Zou, X. *et al.*, A raytracing operator and its adjoint for the use of GPS/MET refraction angle measurements. *J. Geophys. Res*., 1999, **104**, 22301–22318.
8. Liu, H. and Zou, X., Improvements to GPS radio occultation raytracing model and their impacts on assimilation of bending angle. *J. Geophys. Res. D*, 2003, **108**, 4548, JD003160.
9. Healy, S. B., Jupp, A. M. and Marquardt, C., Forecast impact experiment with GPS radio occultation measurements. *Geophys. Res. Lett.*, 2005, **32**, L03804, GL020806.
10. Chen, S. Y., Huang, C. Y., Kuo, Y. H., Guo, Y. R. and Sokolovskiy, S., Typhoon predictions with GPS radio occultation data assimilations by WRF-VAR using local and nonlocal operators. *Terr. Atmos. Ocean. Sci*., 2009, **20**, 133–154.
11. Cucurull, L., Kuo, Y. H., Barker, D. and Rizvi, S. R. H., Assessing the impact of simulated COSMIC GPS radio occultation data on weather analysis over the Antarctic: a case study. *Mon. Weather Rev*., 2006, **134**, 3283–3296.
12. Kuo, Y. H., Sokolovskiy, S. V., Anthes, R. A. and Vandenberghe, F., Assimilation of GPS radio occultation data for numerical weather prediction. *Terr. Atmos. Ocean. Sci*., 2000, **11**, 157–186.
13. Huang, C.-Y., Kuo, Y.-H., Chen, S.-H. and Vandenberghe, F., Improvements on typhoon forecast with assimilated GPS occultation refractivity. *Weather Forecast.*, 2005, **20**, 931–953.
14. Huang, C. Y., Kuo, Y. H. and Chen, S. Y., The assimilation of GPS radio occultation data and its impact on rainfall prediction along the west coast of India during monsoon 2002. *Pure Appl. Geophys*., 2007, **164**, 1577–1591.
15. Huang, C. Y. *et al.*, Impact of GPS radio occultation data assimilation on regional weather predictions. *GPS Solut.*, 2010, **14**, 35–49; doi:10.1007/s10291-009-0144-1.
16. Cucurull, L. and Derber, J. C., Operational implementation of COSMIC observations into NCEP's global data assimilation system. *Weather Forecast.*, 2008, **23**, 702–711.
17. Cucurull, L., Improvement in the use of an operational constellation of GPS radio occultation receivers in weather forecasting. *Weather Forecast.*, 2010, **25**, WAF2222302.1.
18. Cucurull, L., Derber, J. C. and Purser, R. J., A bending angle forward operator for global positioning system radio occultation measurements. *J. Geophys. Res. Atmos.*, 2013, **118**, 14–28, 2012JD017782.
19. Smith, E. K. and Weintraub, S., The constants in the equation for atmospheric refractivity index at radio frequencies. *Proc. IRE*, 1953, **41**, 1035–1037.
20. Developmental Testbed Center, Gridpoint Statistical Interpolation (GSI) User's Guide for Version 3.0, 2011; http://www.dtcenter.org/com-GSI/users/docs/
21. Prasad, V. S., Mohandas, S., Das Gupta, M., Rajagopal, E. N. and Dutta, S. K., Implementation of upgraded global forecasting systems (T382L64 and T574L64) at NCMRWF. NCMRWF/TR/5/2011, 2011; http://www.ncmrwf.gov.in/ncmrwf/gfs_report_final.pdf
22. Dutta, S. K. and Prasad, V. S., Impact of gridpoint statistical interpolation scheme over Indian region. *J. Earth Syst. Sci*., 2011, **120**(6), 1095–1112.
23. Kleist, D. T., Parrish, D. F., Derber, J. C., Treadon, R. Wu, W.-S. and Lord, S., Introduction of the GSI into the NCEP global data assimilation system. *Weather Forecast.*, 2009, **24**, 1691–1705.
24. Cucurull, L., Derber, J. C. and Lapenta, W., Assessing the benefits of assimilating GPS RO profiles into global numerical weather prediction models. WMO workshop, Sedona, Arizona, USA, 2012.
25. Cucurull, L., Derber, J. C., Treadon, R. and Purser, R. J., Assimilation of global positioning system radio occultation observations into NCEP's global data assimilation system. *Weather Forecast.*, 2007, **135**, MWR3461.1.
26. Chien, F. C. and Kuo, Y. H., Impact of FORMOSAT-3/COSMIC GPS radio occultation and drop windsonde data on regional model predictions during the 2007 Mei-yu season. *GPS Solut.*, 2010, **14**, 51–63, DOI: 10.1007/s10291-009-0143-2.

ACKNOWLEDGEMENTS. We thank the Director, NCMRWF, Noida for support and encouragement. We also thank Mr Harvir Singh, NCMRWF, Noida for help while using the model verification package MET.

Received 27 August 2013; revised accepted 13 March 2014